Synergism between Gradient Dilution Work Function and Janus Electronic State of Pt-CoP_xBr_{1-x} for Boosting Alkaline Seawater electrolysis

Lei Jin, Hui Xu, Kun Wang, Yang Liu, Jie Chen, Xingyue Qian, Haiqun Chen, Guangyu He**

Key Laboratory of Advanced Catalytic Materials and Technology, Advanced Catalysis and Green Manufacturing Collaborative Innovation Center, Changzhou University, Changzhou, Jiangsu Province 213164, China

Corresponding authors: xuhui006@cczu.edu.cn (H. Xu); chenhq@cczu.edu.cn (H. Chen); hegy@cczu.edu.cn (G. He)

1. Material Characterizations

Crystalline structures were analyzed using powder X-ray diffraction (pXRD, D8, Bruker AXS) with Cu Kα radiation (λ = 1.5418 Å). The microstructures of the products were observed by transmission electron microscopy (TEM, JEM-2100F) and field-emission scanning electron microscopy (FESEM, Zeiss Supra 55) that equipped with element mappings. The morphologies of the materials were characterized by scanning electron microscopy (SEM, Zeiss Sigma 300 Cold Field scanning electron microscope). X-ray photoelectron spectroscopy (XPS, PHI-5000C ESCA, PerkinElmer, USA) was employed to obtain elemental information of prepared catalysts on a VG ESCALAB MKII using Al Ka radiation. Ultraviolet photoelectron spectroscopy (UPS) is performed on Thermo ESCALAB Xi+ equipped with ultraviolet photoelectron spectrometer (Hel (21.22 eV)). Electron paramagnetic resonance (EPR) spectra were recorded on a Bruker EPR ELEXSYS 500 spectrometer. Absorbance data of spectrophotometer were measured on UV-2700 spectrophotometer. Analysis of the molecular structure of the catalyst was performed using a Raman spectrometer (XPOLORA PLUS, China) at an excitation wavelength of 532 nm for Raman scattering peak analysis.

2. Electrochemical Measurements

All the electrochemical measurements were tested using a CHI760E electrochemical workstation with a standard three electrode cell. The reference and counter electrodes were Hg/HgO and graphite rod, respectively. A glassy carbon electrode (GCE. 5 mm inner diameter, 0.196 cm^2 area) that modified with catalyst ink is used as the working electrode. The homogeneous catalyst ink was made by ultrasonically dispersing a mixture containing 2 mg of catalyst, 20 μL Nafion (5 wt%), 360 μL ethanol and 120 μL H_2O. Then, 13 μL of the catalyst ink was dropped on the surface of GCE with an approximate mass loading of 265.0 $\mu g \cdot cm^{-2}$. All potentials were measured against Hg/HgO and converted to reversible hydrogen electrode (RHE) by Nernst equation: $E_{vs\ RHE} = E_{vs\ Hg/HgO} + 0.0591 \cdot pH + 0.098$. The overpotential (η) was calculated through the formula: $\eta = E_{RHE} - 1.23$ V. Cyclic Voltammograms (CV) were measured at a scan rate of 5 $mV \cdot s^{-1}$. Electrochemical impedance spectroscopy was

tested over the frequency range of 10^6 to 10^{-2} Hz with an AC signal amplitude of 5 mV. The double-layer capacitance (C_{dl}) was evaluated by cyclic voltammetry (CV) curves performed at the non-faraday reaction regions with an interval of 20 mV·s^{-1} over the scanning range of 20 ~ 120 mV·s^{-1}. The turnover frequency (TOF) values were calculated from the following equation: TOF (s^{-1}) = (j × A)/ (k × F × n). Here, k is the number of electron transfer (the factors of HERis 2), j is the current density at a given overpotential, A is the geometric surface area of the electrode, F is the Faraday constant (96485.3 C mol^{-1}), n is the number of active sites (mol). The number of voltammetric charges is gained by CV curves from 0 ~ 0.6 V *vs*. RHE for HER in a phosphate buffer solution (pH = 7) with a scan rate of 50 mV s^{-1} respectively, and the following equation is n (mol) = Q/2F (the surface charge Q is proportional to the number of active sites). The long-term stability of the catalyst was conducted by chronopotentiometry (CP). All the data of electrochemistry were presented without any i*R* correction. In situ electrochemistry-Raman coupled experiments were conducted in a single-compartment, three-electrode, custom-made quartz cell controlled by an electrochemical workstation at room temperature. The loaded GCE, a graphite rod, and SCE were used as the working, counter, and reference electrodes, respectively. A stability potential in the range of -0.09468 to -1.0268 V with an interval of 0.02 V was applied to the catalyst electrode for 5 min before carrying out all in situ Raman spectra.

3. Finite Element Simulations

Free electron density and electric field around electrode were simulated using the COMSOL multiphysics finite-element-based solver. The "Electrostatics" module was used to simulate electric field when the electrode is under a specific potential bias. The electric field, E, was computed as the negative gradient of the electric potential as follows:

$$E = -\nabla V$$

The simulation model for Pt nanoparticles was a cone table with 2, 5, and 30 nm for top radii, bottom radii, and cone height, respectively. The electric potentials -1.5 V was applied to the bottom of the needle. The ground was prescribed to the far side of

the electrolyte. Electric insulation was applied to the remaining electrolyte sides, and an initial value of 0 V was set everywhere.

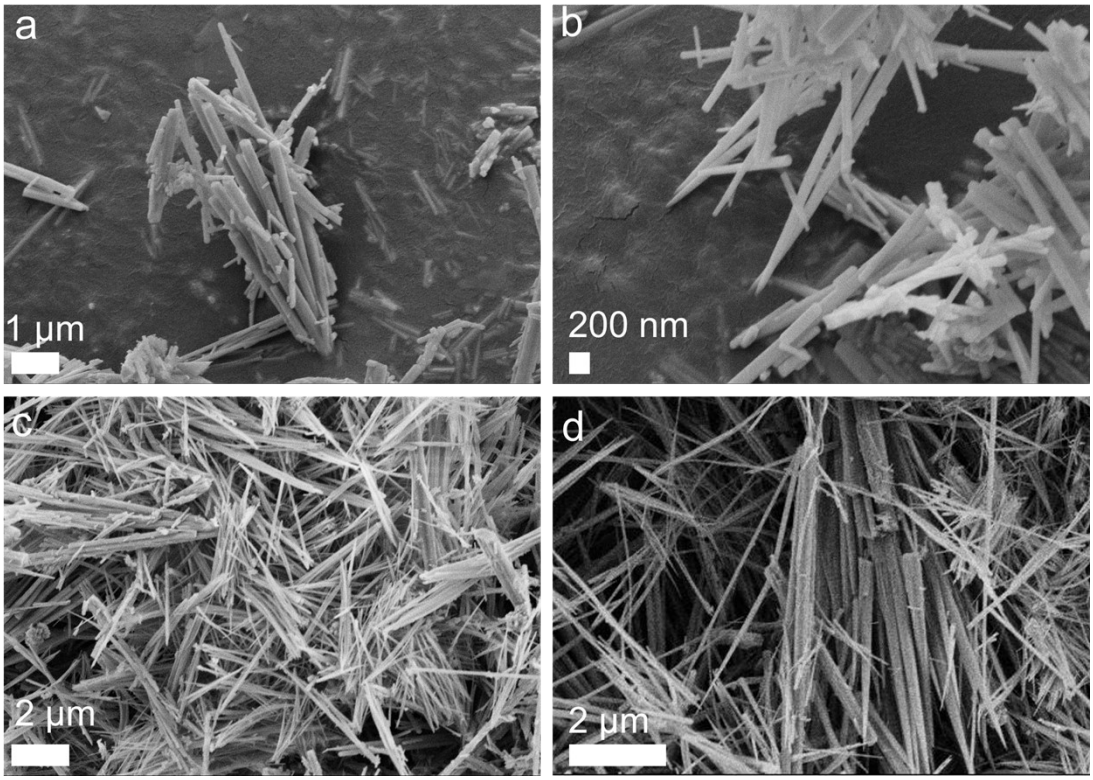

Fig. S1 SEM image of the CoP, CoP_xBr_{1-x}, Pt-CoP and Pt-CoP_xBr_{1-x}.

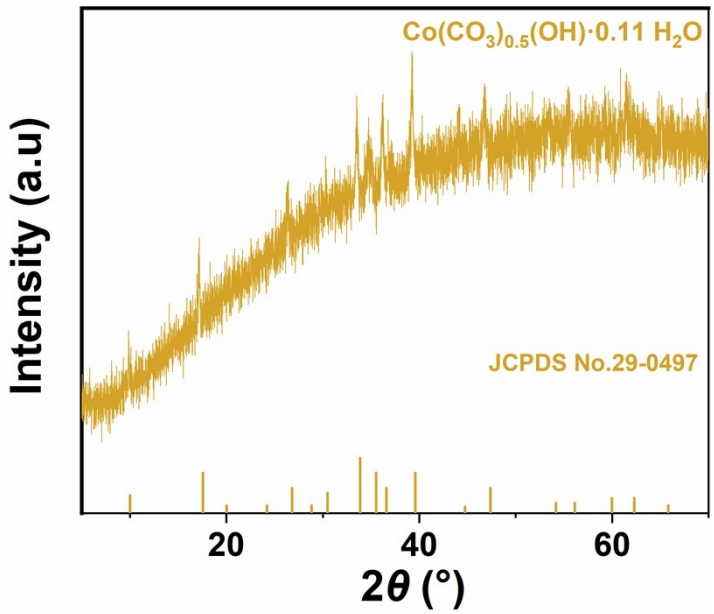

Fig. S2 XRD pattern of the $Co(CO_3)_{0.5}(OH)\cdot 0.11H_2O$.

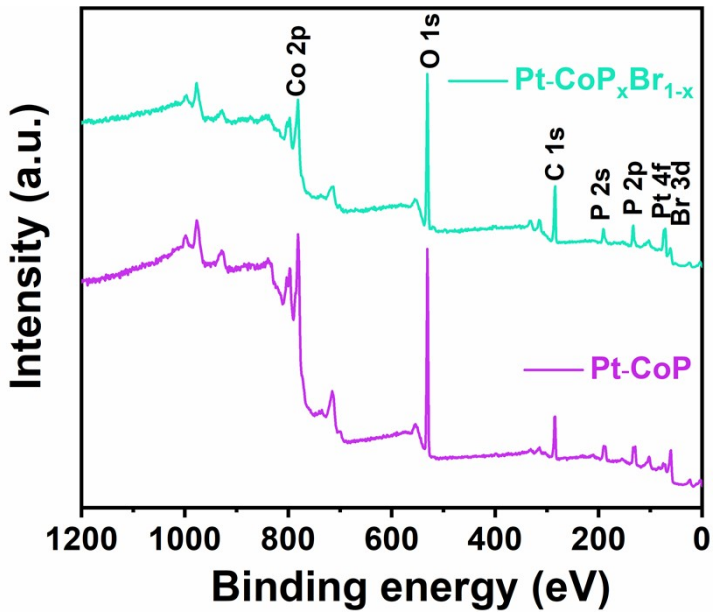

Fig. S3 XPS survey spectra of the Pt-CoP and Pt-CoP_xBr_{1-x}.

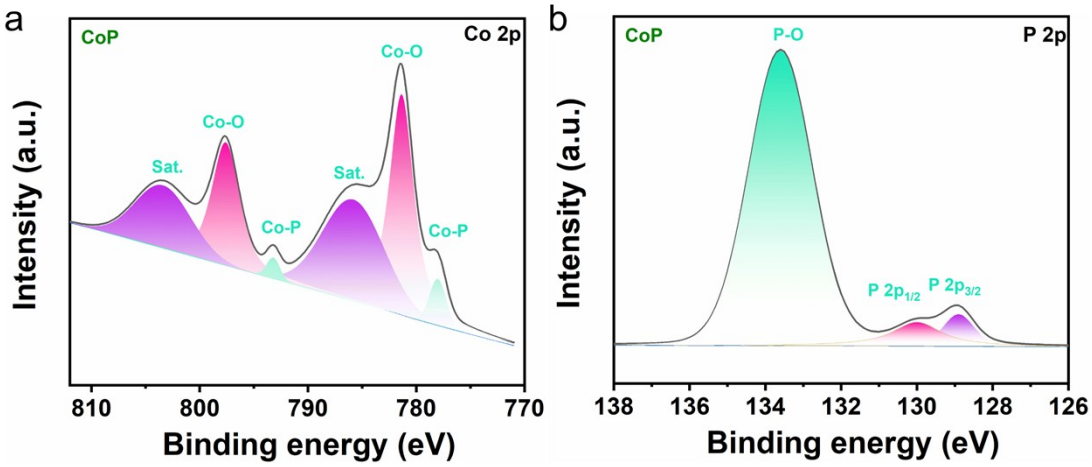

Fig. S4 High-resolution (a) Co 2p and (b) P 2p XPS spectra of CoP.

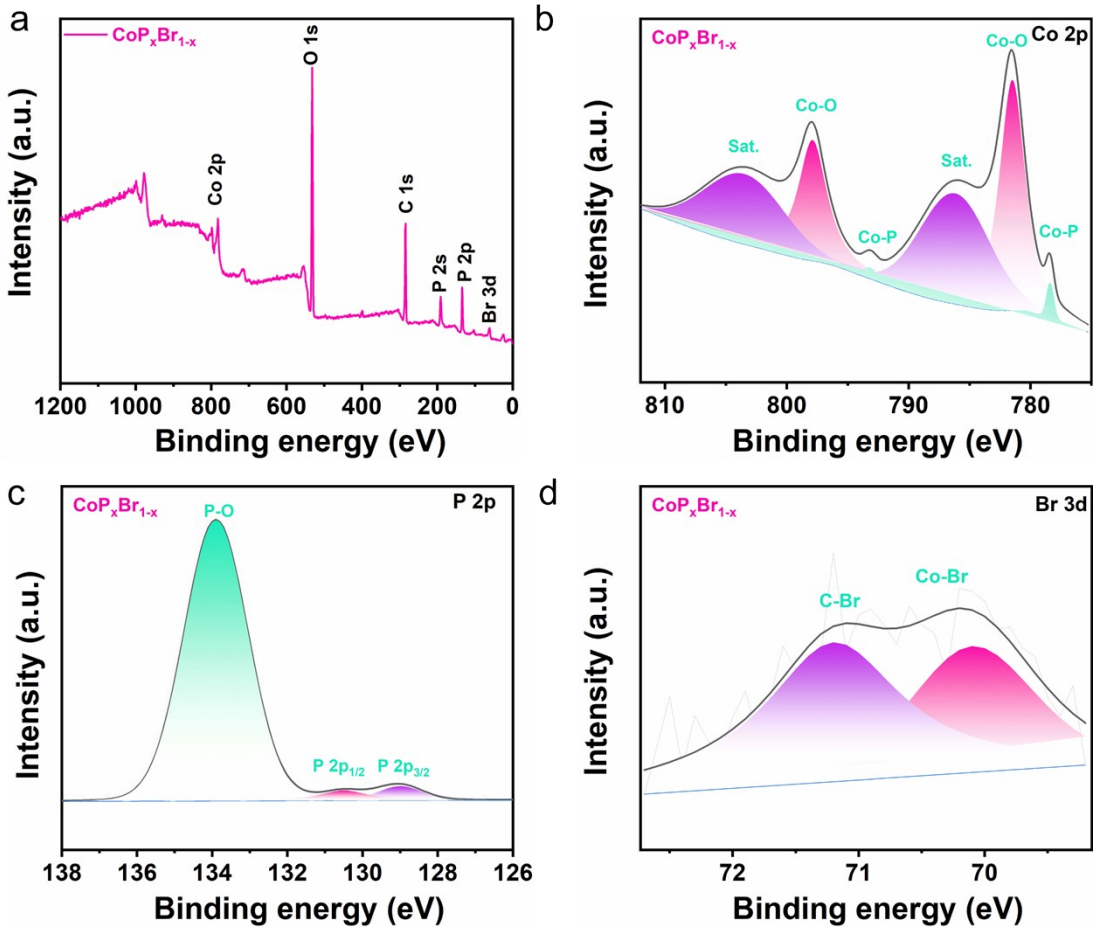

Fig. S5 (a) XPS survey spectra, High-resolution (b) Co 2p, (c) P 2p (d) Br 3d XPS spectra of CoP_xBr_{1-x}.

Table S1. UPS measured work functions of as-prepared catalysts

Catalysts	E_{cutoff} (eV)	E_{VB} (eV)	Φ (eV)
CoP	15.34	3.3	5.88
CoP_xBr_{1-x}	15.48	3.46	5.74
Vp-CoP_xBr_{1-x}	15.61	3.41	5.61
Pt	15.79	-----	5.43

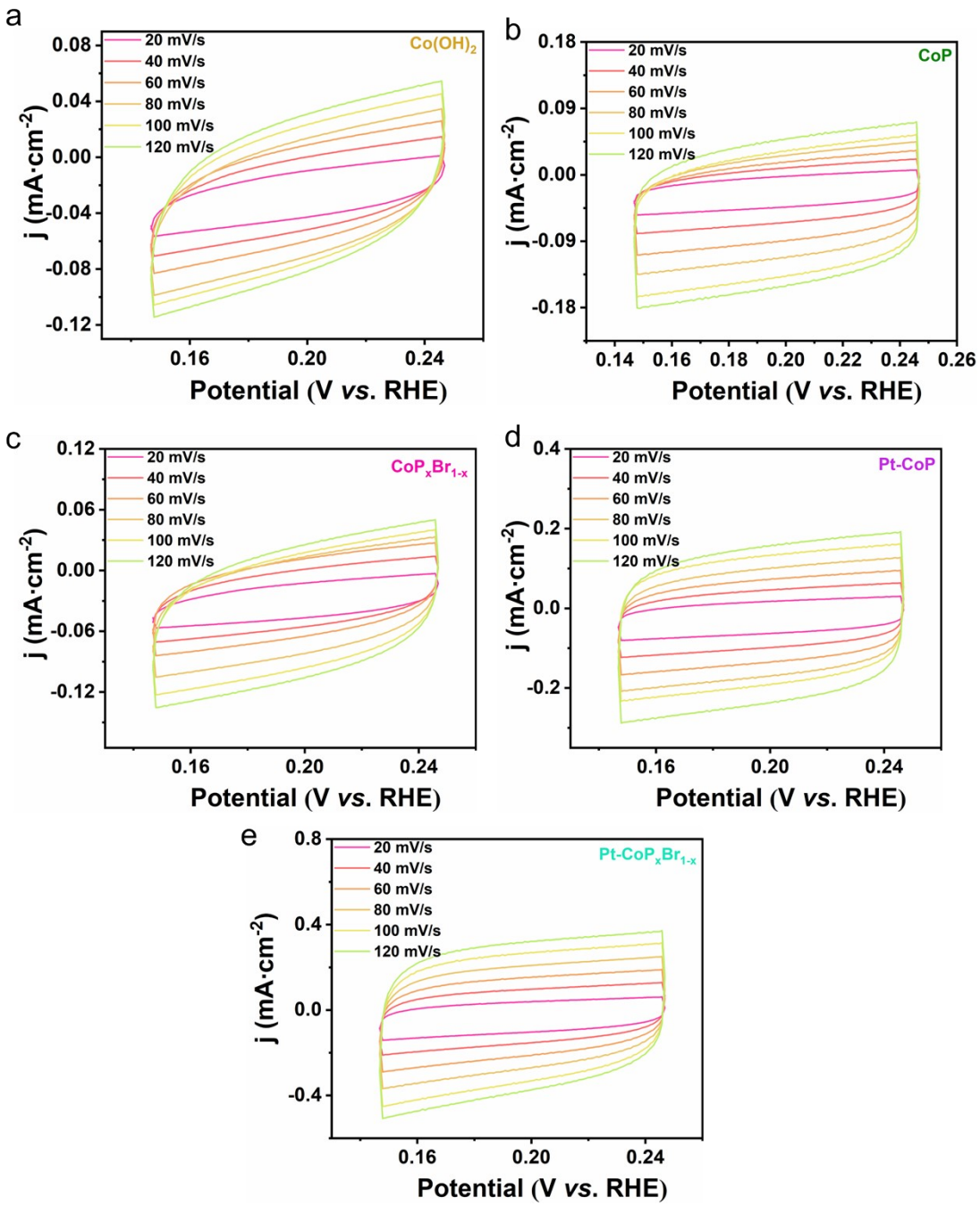

Fig. S6 (a-e) CV curves of different electrocatalysts with different scanning rates for HER in alkaline seawater solution.

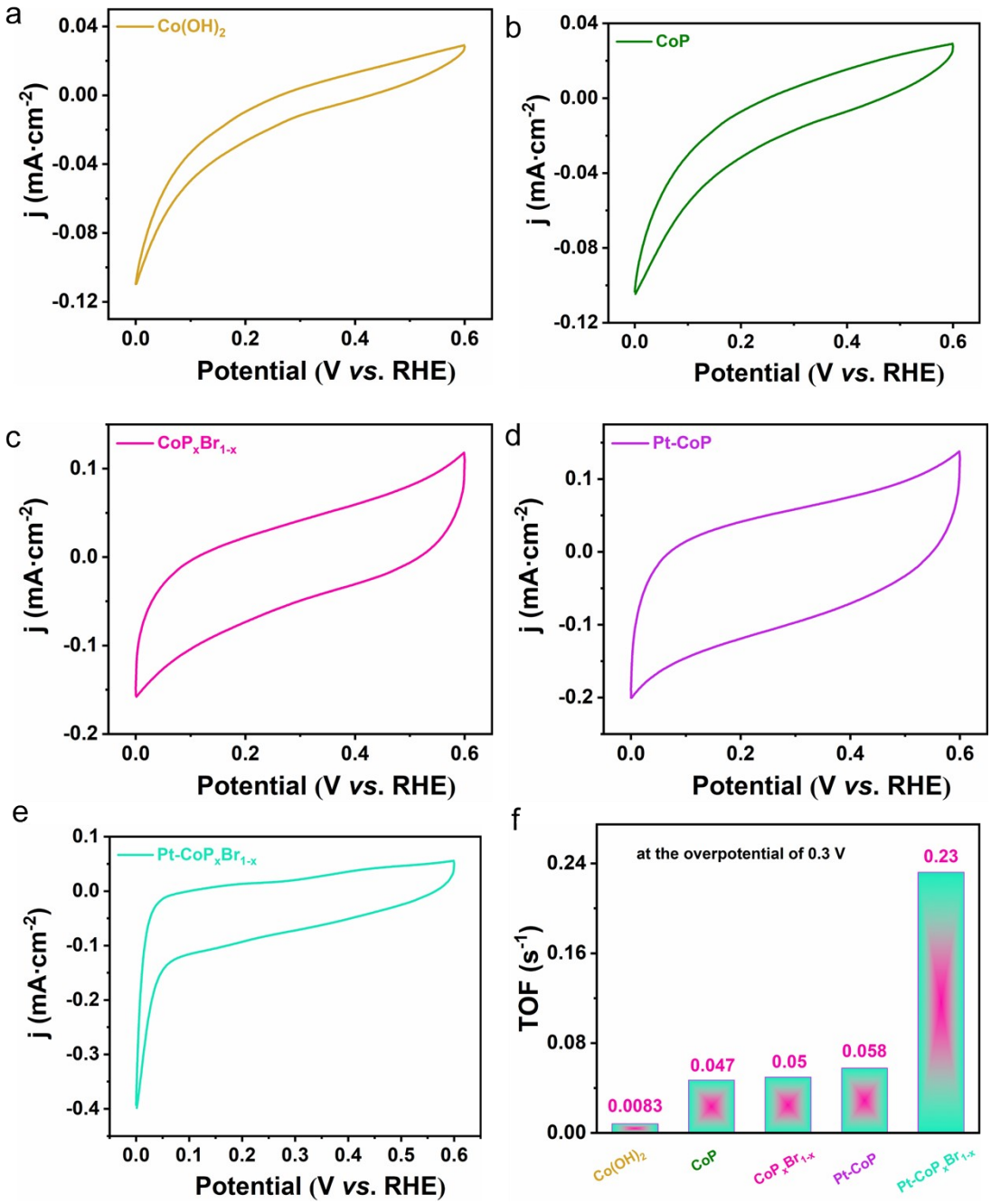

Fig. S7 (a-e) CV curves from 0 to 0.6 V *vs.* RHE for HER in 1.0 M PBS (pH = 7) at 50 mV s^{-1}. f) TOF values of different catalysts for HER in alkaline seawater solution.

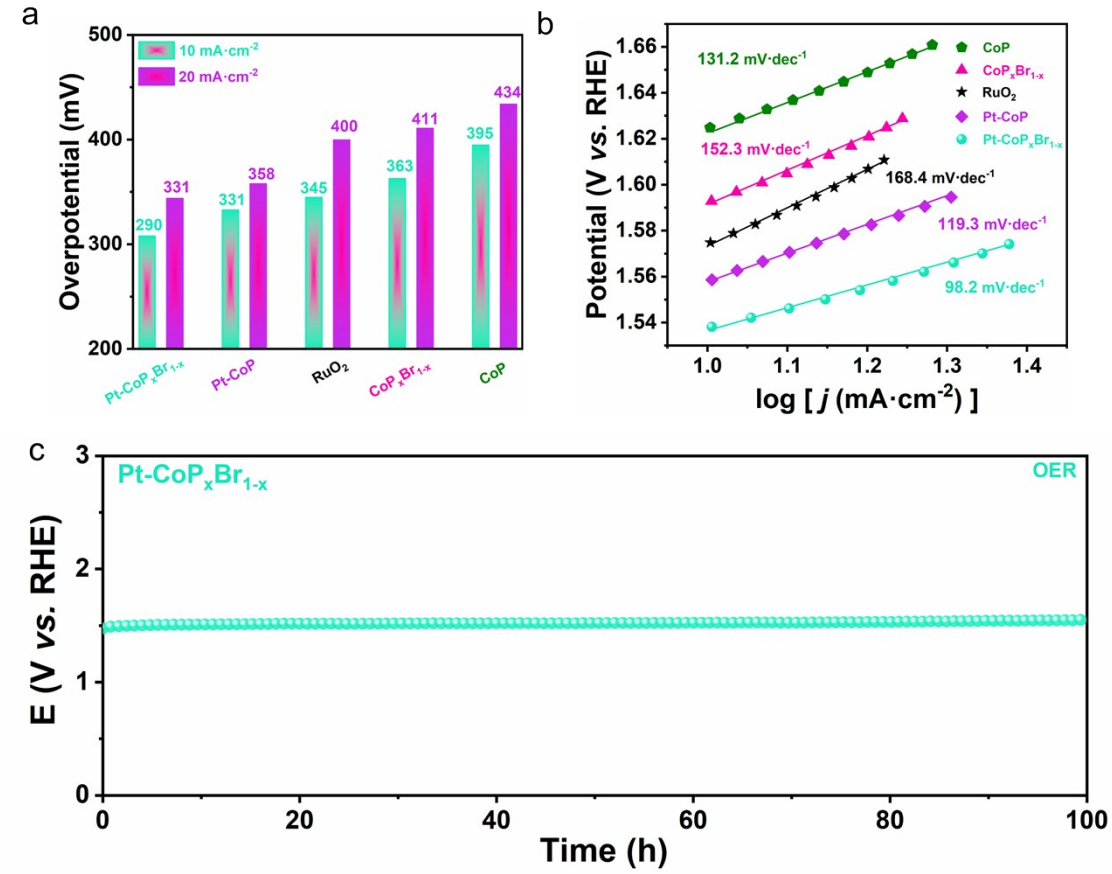

Fig. S8 OER performance of Pt-CoP_xBr_{1-x} and referenced samples. (a) Histograms of the overpotentials at 10 mA cm^{-2} and 20 mA cm^{-2}. (b) Tafel plots. (c) CP test of Pt-CoP_xBr_{1-x} at a constant current density of 10 mA cm^{-2}.

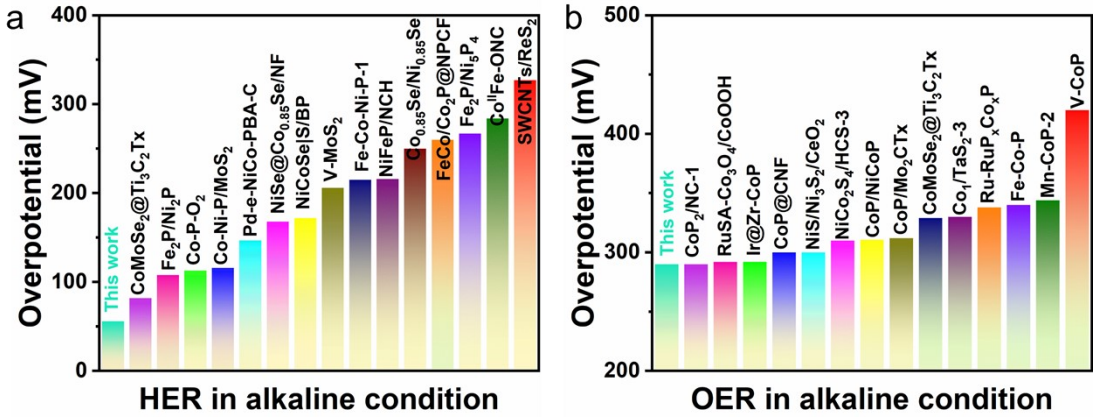

Fig. S9 (a, b) Comparison of Pt-CoP_xBr_{1-x} with reported HER and OER electrocatalysts in an alkaline condition at 10 mA·cm^{-2}.

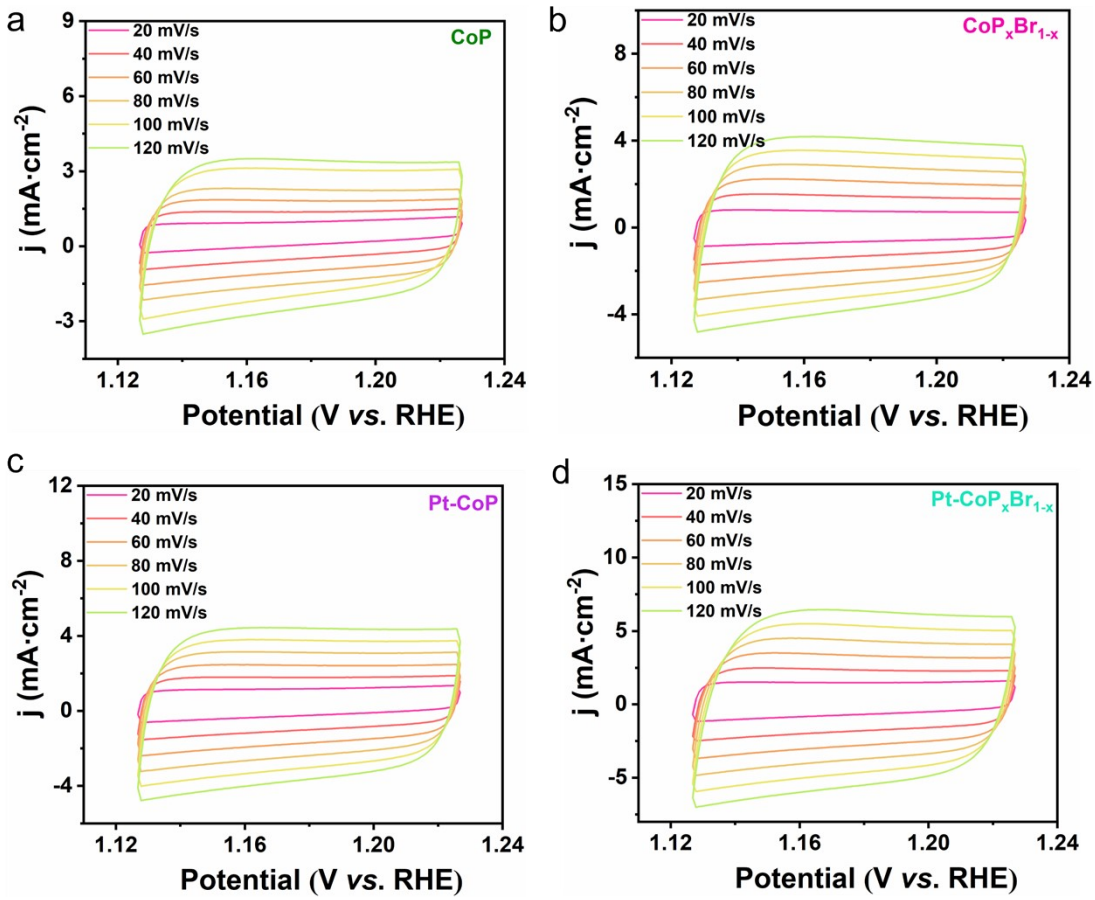

Fig. S10 (a-d) CV curves of different electrocatalysts with different scanning rates for OER in alkaline seawater solution.

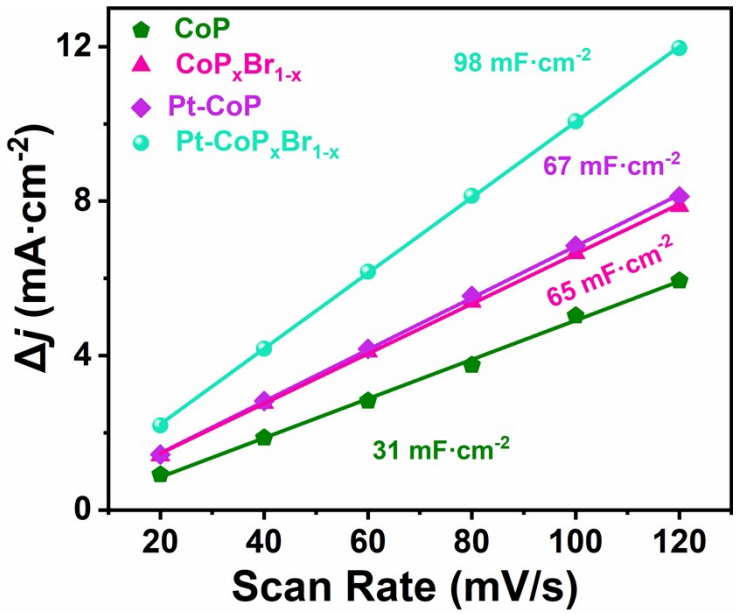

Fig. S11 C_{dl} values of different catalysts for OER in alkaline seawater solution.

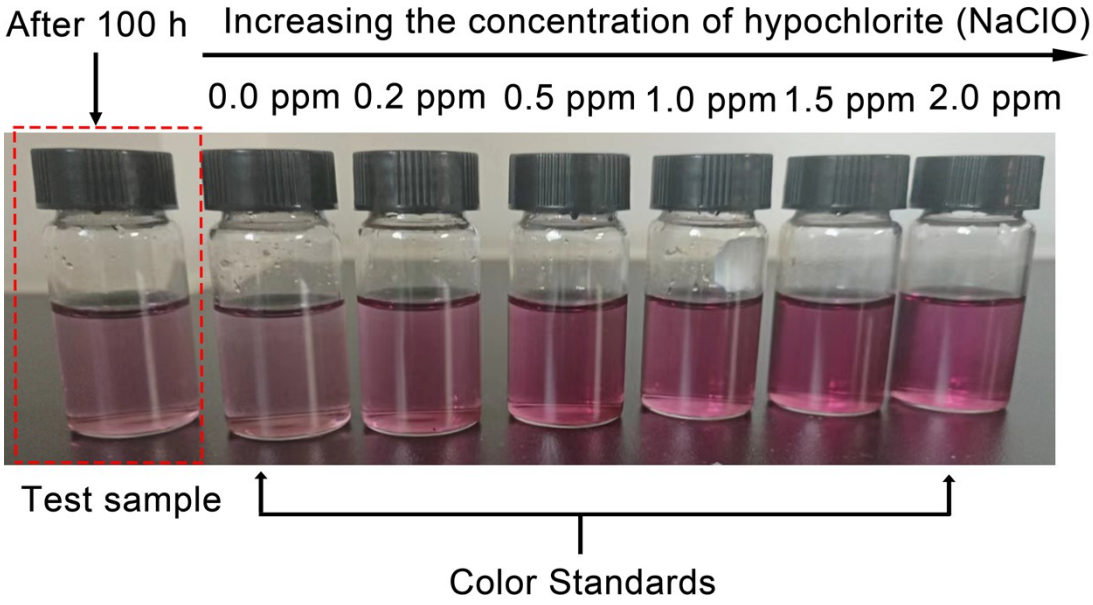

Fig. S12 Hypochlorite detection result with different NaClO contents and the electrolyte after 100 h electrolysis for Pt-CoP_xBr_{1-x} at a constant current density of 10 mA cm^{-2} in 1 M KOH + seawater.

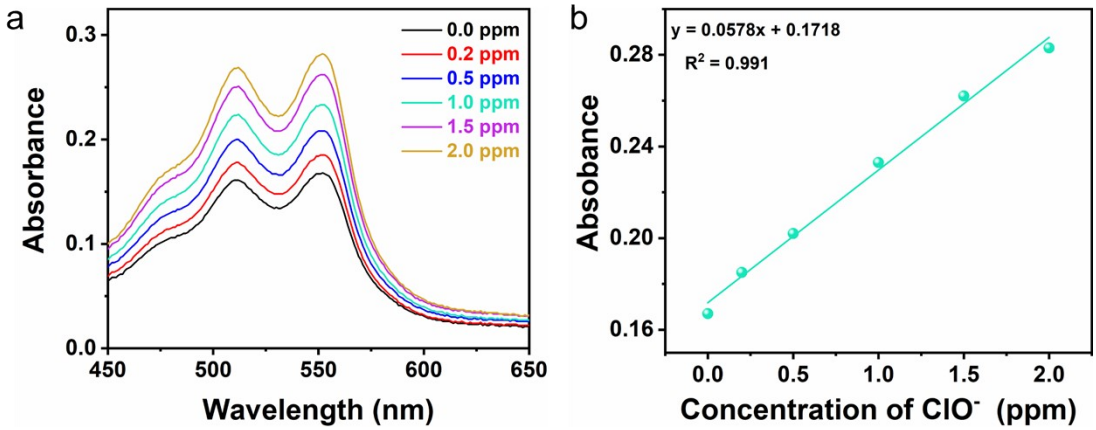

Fig. S13 (a) UV-Vis absorption spectra of ClO^- with different concentrations. (b) Calibration curve used for calculating ClO^- concentrations of the electrolyte.

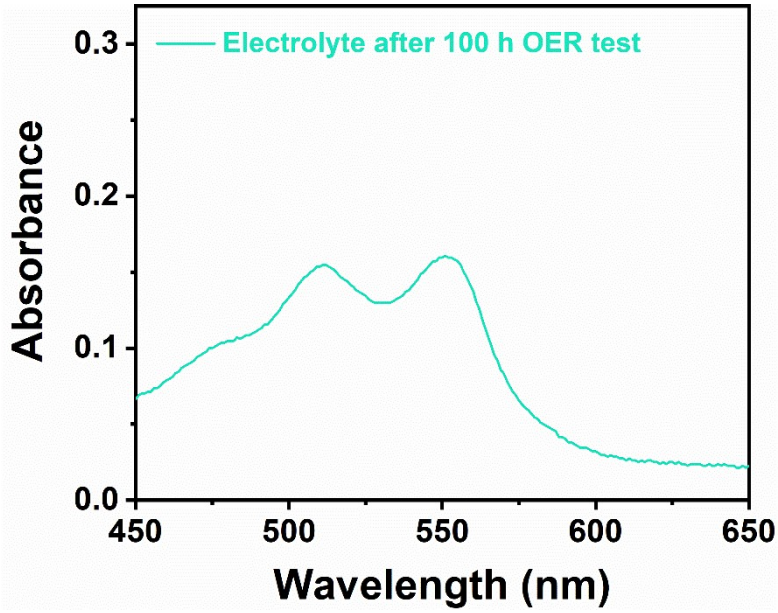

Fig. S14 UV/Vis absorption spectrum of the electrolyte after 100 h electrolysis for Pt-CoP_xBr_{1-x} at a constant current density of 10 mA cm^{-2} in 1 M KOH + seawater.

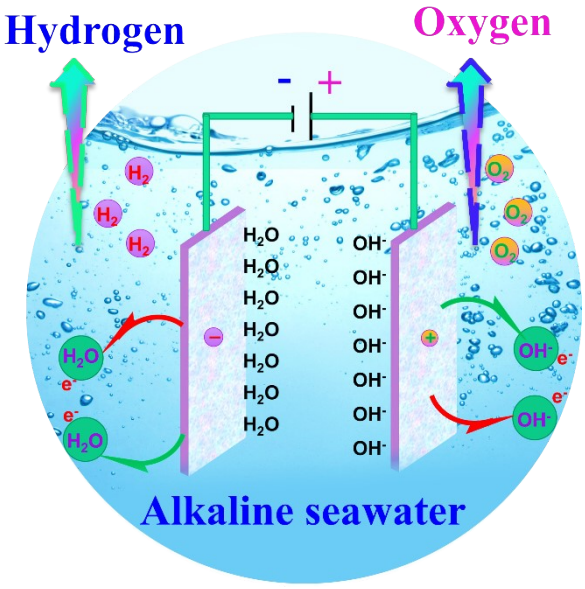

Fig. S15 A schematic illustration of the electrolyzer using Pt-CoP_xBr_{1-x} as the cathode and the anode.

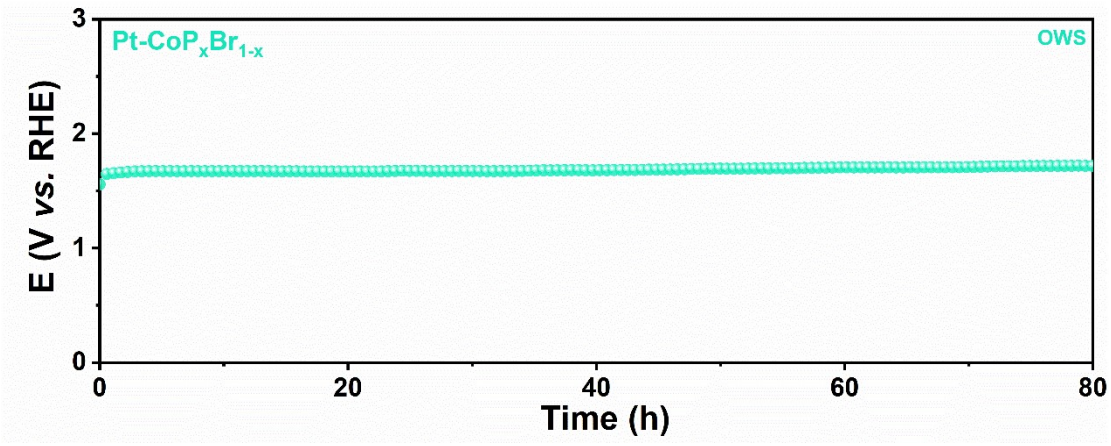

Fig. S16 Long-term stability plot of Pt-CoP$_x$Br$_{1-x}$|| Pt-CoP$_x$Br$_{1-x}$ at 10 mA cm^{-2} in 1 M KOH + seawater.

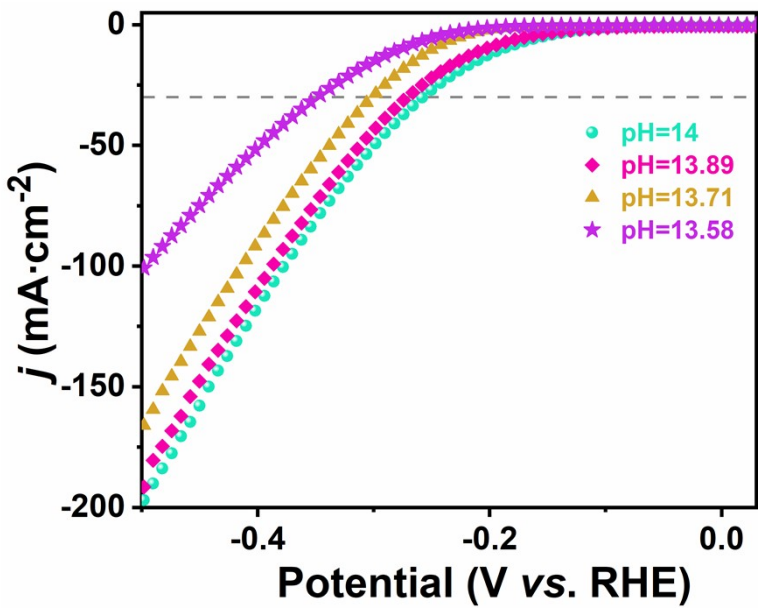

Fig. S17 HER performance of Pt-CoP in alkaline seawater electrolyte with various pH.

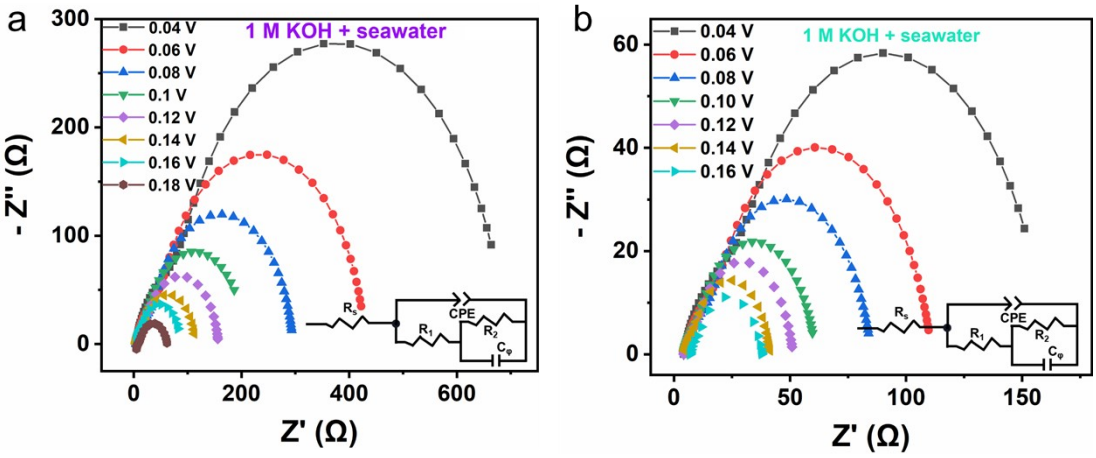

Fig. S18 (a, b) EIS curves of Pt-CoP and Pt-CoP_xBr_{1-x} for HER in alkaline seawater solution.

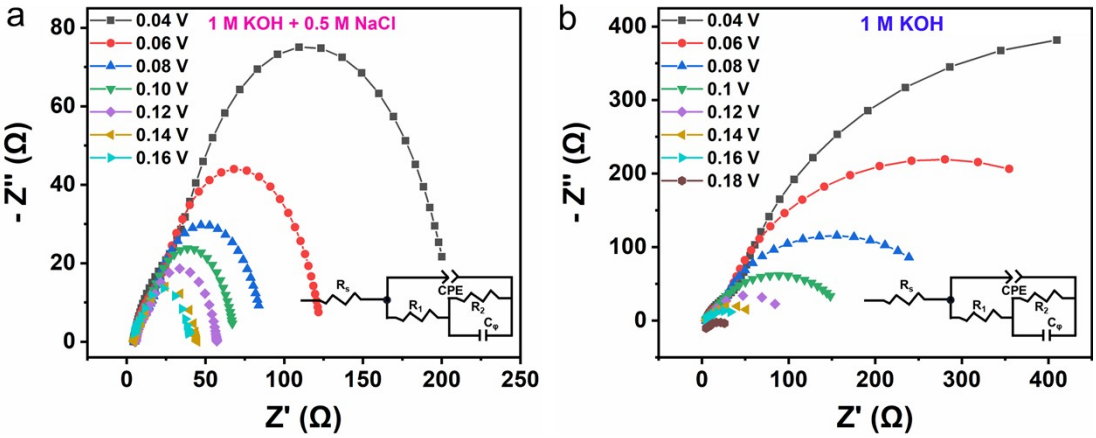

Fig. S19 (a, b) EIS curves of Pt-CoP_xBr_{1-x} for HER in 1 M KOH and 1 M KOH + 0.5 M NaCl.

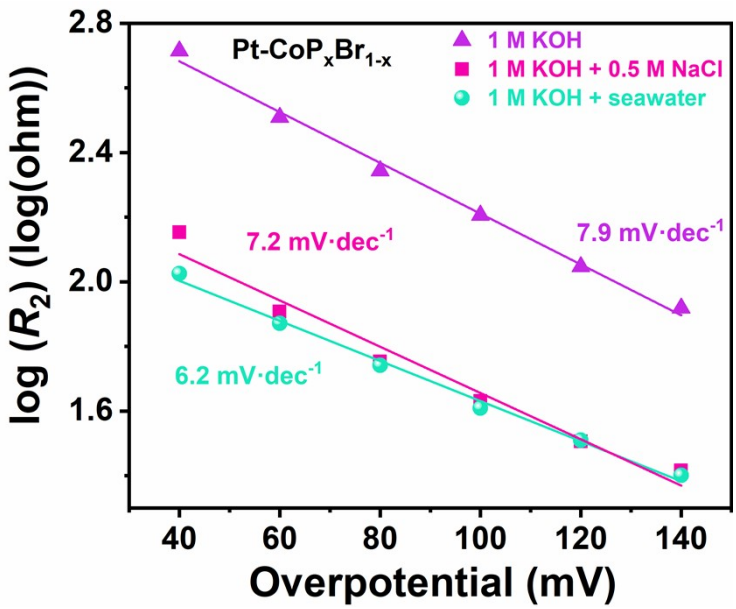

Fig. S20 EIS-derived Tafel plots of the Pt-CoP_xBr_{1-x} samples attained from the hydrogen adsorption resistance R_2 in various solutions.

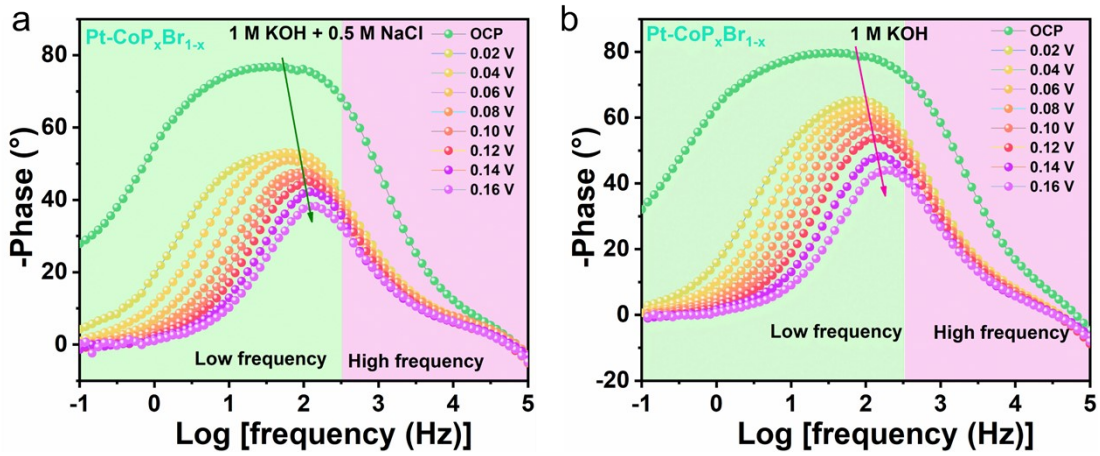

Fig. S21 (a, b) Phase angles of Pt-CoP_xBr_{1-x} in 1 M KOH + 0.5 M NaCl and 1 M KOH.

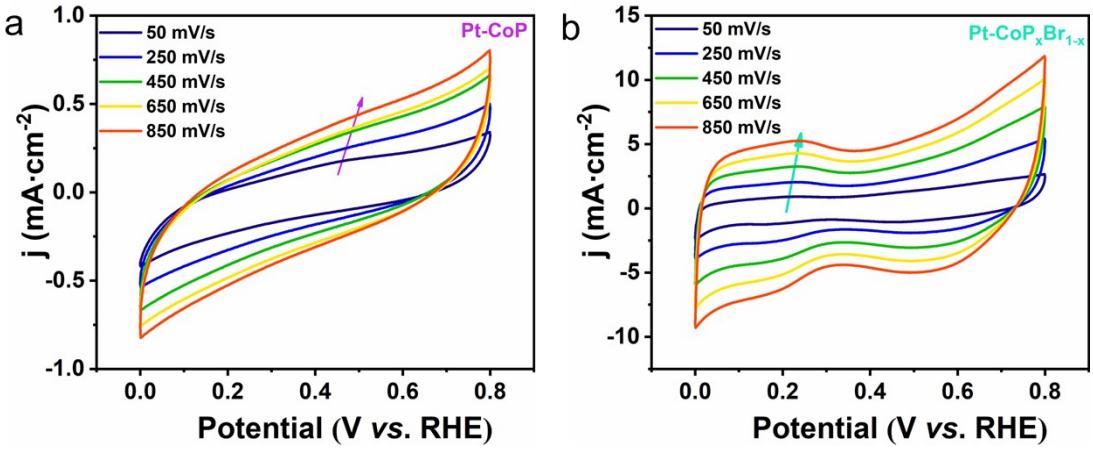

Fig. S22 (a, b) Cyclic voltammetry curves of Pt-CoP and Pt-CoP_xBr_{1-x}.

Table S2 Comparison of HER performance in alkaline solution using Pt-CoP_xBr_{1-x} and other reported electrocatalysts.

Catalysts	Overpotential (mV)	Current density (mA cm^{-2})	Ref
Pt-CoP_xBr_{1-x}	**56**	**10**	**This work**
$CoMoSe_2$@$Ti_3C_2T_x$	82	10	1
Fe_2P/Ni_2P	108	10	2
Co-P-O_2	113	10	3
Co-Ni-P/MoS_2	116	10	4
Pd-e-NiCo-PBA-C	147	10	5
NiSe@$Co_{0.85}Se$/NF	168	10	6
NiCoSe|S/BP	172	10	7
V-MoS_2	206	10	8
Fe-Co-Ni-P-1	215	10	9
NiFeP/NCH	216	10	10
$Co_{0.85}Se/Ni_{0.85}Se$	250	10	11
FeCo/Co_2P@NPCF	260	10	12
Fe_2P/Ni_5P_4	267	10	13
Co^{II}Fe-ONC	284	10	14
SWCNTs/ReS_2	327	10	15

Table S3 Comparison of OER performance in alkaline solution using Pt-CoP_xBr_{1-x} and other reported electrocatalysts.

Catalysts	Overpotential (mV)	Current density (mA cm^{-2})	Ref
Pt-CoP_xBr_{1-x}	**290**	**10**	**This work**
CoP_2/NC-1	290	10	3
Ru_{SA}-Co_3O_4/CoOOH	292	10	16
Ir@Zr-CoP	292	10	17
CoP@CNF	300	10	18
NiS/Ni_3S_2/CeO_2	300	10	19
$NiCo_2S_4$/HCS-3	310	10	20
CoP/NiCoP	310.7	10	21
CoP/Mo_2CT_x	312	10	22
$CoMoSe_2$@$Ti_3C_2T_x$	329	10	23
Co_1/TaS_2-3	330	10	24
Ru-RuP_xCo_xP	338	10	25
Fe-Co-P	340	10	26
Mn-CoP-2	344	10	27
V-CoP	420	10	28

Table S4 The alkaline OWS performance of Pt-CoP_xBr_{1-x} with some representative bifunctional electrocatalysts reported.

Catalysts	Electrolyte	Cell voltage (V)	Ref
Pt-CoP_xBr_{1-x}	**1.0 KOH+ Seawater**	**1.62**	**This work**
CoNSC	1.0 KOH	1.64	29
CoP@SNC	1.0 KOH	1.64	30
v- NiS_2/CeO_2	1.0 KOH	1.64	31
$NiCo_2O_4$	1.0 KOH	1.65	32
Co-NC/C	1.0 KOH	1.67	33
NiFe LDH/NF	1.0 KOH	1.7	34
Ni_5Ni_4/NF	1.0 KOH	1.7	35
Ni_3S_2	1.0 KOH	1.76	36

Table S5 The fitted parameters of the EIS data of Pt-CoP_xBr_{1-x} and Pt-CoP for HER in alkaline seawater.

Catalysis	η (mV)	Rs (Ω)	R_1 (Ω)	$C_φ$ (F)
	-40	4.186	106.1	0.522
	-60	4.358	74.49	0.588
	-80	4.348	55.15	0.591
Pt-CoP_xBr_{1-x}	-100	4.198	40.71	0.682
	-120	4.243	32.36	1.28
	-140	4.172	25.17	1.451
	-40	4.747	517.7	0.130
	-60	4.746	322.8	0.130
	-80	4.795	220.5	0.137
Pt-CoP	-100	4.738	160.7	0.148
	-120	4.764	111.4	0.158
	-140	4.794	82.93	0.187

Table S6 The fitted parameters of the EIS data of Pt-CoP_xBr_{1-x} for HER in 1 M KOH + 0.5 M NaCl and 1 M KOH.

Electrolyte	η (mV)	Rs (Ω)	R_1 (Ω)	$C_φ$ (F)
	-40	4.155	142.3	0.413
	-60	4.425	80.84	0.438
	-80	4.567	56.64	0.440
1 M KOH + 0.5 M NaCl	-100	4.552	42.75	0.465
	-120	4.577	32.05	0.516
	-140	4.623	26.08	0.62
	-40	4.202	462.6	0.272
	-60	4.392	243.6	0.291
	-80	4.5	131.9	0.407
1 M KOH	-100	4.655	76.34	0.422
	-120	4.637	45.75	0.501
	-140	4.667	28.25	0.605

References

1. J. J. J. J. Kamaraj, A. K. Ravindran, S. P. Muthu and R. Perumalsamy, *J. Power Sources*, 2025, **629**, 235951

2. L. Jin, H. Xu, K. Wang, Y. Liu, X. Qian, H. Chen and G. He, *Chem. Sci.* 2025, **16**, 329-337.

3. Y. Chen, Z. Yang, J. Wang, Y. Yang, X. He, Y. Wang, J. Chen, Y. Guo, X. Wang, S. Wang, *Nano Res.* 2023, **1**.

4. Q. P. Ngo, T. T. Nguyen, Q. T. T. Le, J. H. Lee, N. H. Kim, *Adv. Energy Mater.* 2023, **13**, 2301841.

5. R. Zhang, Z. Wei, G. Ye, G. Chen, J. Miao, X. Zhou, X. Zhu, X. Cao, X. Sun, *Adv. Energy Mater*. 2021, **11**, 2101758.

6. A. Ren, B. Yu, M. Huang, Z. Liu, *I Int. J. Hydrogen Energy.* 2024, **51**, 490.

7. C. Lyu, C. Cao, J. Cheng, Y. Yang, K. Wu, J. Wu, W.-M. Lau, P. Qian, N. Wang, J. Zheng, *Chem. Eng. J*. 2023, **464**, 142538.

8. M. Bi, Y. Zhang, X. Jiang, J. Sun, X. Wang, J. Zhu, Y. Fu, *Adv. Energy Mater.* 2024, **34**, 2309330.

9. J.-B. Chen, J. Ying, Y.-X. Xiao, G. Tian, Y. Dong, L. Shen, S. I. Córdoba de Torresi, M. D. Symes, C. Janiak, X.-Y. Yang, *ACS Catal*. 2023, **13**, 14802.

10. S. Liu, Z. Lin, R. Wan, Y. Liu, Z. Liu, S. Zhang, X. Zhang, Z. Tang, X. Lu, Y. Tian, *J. Mater. Chem.* A. 2021, **9**, 21259.

11. X. Fu, Z. Zhang, Y. Zheng, J. Lu, S. Cheng, J. Su, H. Wei, Y. Gao, *J. Colloid Interf. Sc*i. 2024, **653**, 1272.

12. L. Wang, Q. Zhou, Z. Pu, Q. Zhang, X. Mu, H. Jing, S. Liu, C. Chen, S. Mu, *Nano Energy.* 2018, **53**, 270.

13. L. Jin, H. Xu, K. Wang, Y. Liu, X. Qian, G. He and H. Chen, *J. Mater. Chem. A*, 2024, **12**, 32014-32021.

14. Y. Liu, N. Ran, R. Ge, J. Liu, W. Li, Y. Chen, L. Feng, R. Che, *Chem. Eng. J.* 2021, **425**, 131642.

15. K. Liu, C. Zhang, Y. Sun, G. Zhang, X. Shen, F. Zou, H. Zhang, Z. Wu, E. C. Wegener, C. J. Taubert, *ACS Nano,* **2018**, **12**, 158.

16. J. Bao, Y. Zhou, Y. Zhang, X. Sheng, Y. Wang, S. Liang, C. Guo, W. Yang, T. Zhuang, Y. Hu, *J. Mater. Chem. A*. 2020, **8**, 22181.

17. Y.-r. Hao, H. Xue, J. Sun, N. Guo, T. Song, H. Dong, Z. Zhao, J. Zhang, L. Wu and Q. Wang, *Energy Environ. Sci.*, 2024.

18. S. Bolar, S. Shit, J. S. Kumar, N. C. Murmu, R. S. Ganesh, H. Inokawa, T. Kuila,

19. K. Ao, J. Dong, C. Fan, D. Wang, Y. Cai, D. Li, F. Huang, Q. Wei, *ACS sustainable Chem. Eng*. 2018, **6**, 10952.

*Appl. Catal. B: Environ. Energ*y, 2019, **254**, 432.

20. D. Xiang, Z. Qin, Y. Gan, X. Luo, X. Li, L. Hu, Y. Xin, X. Lv, M. Hu and S. Jiao, *Mater. Today Chem.*, 2023, **34**, 101791.

21. J. Liu, X. Meng, J. Xie, B. Liu, B. Tang, R. Wang, C. Wang, P. Gu, Y. Song and S. Huo, *Adv. Funct. Mater*, 2023, **33**, 2300579.

22. Y.-S. Wei, M. Zhang, M. Kitta, Z. Liu, S. Horike, Q. Xu, *J. Am. Chem. Soc*. 2019, **141**, 7906.

23. Q. Shi, Q. Liu, Y. Ma, Z. Fang, Z. Liang, G. Shao, B. Tang, W. Yang, L. Qin, X. Fang, *Adv. Energy Mater*. 2020, **10**, 1903854.

24. Z. Li, Z. Wang, S. Xi, X. Zhao, T. Sun, J. Li, W. Yu, H. Xu, T. S. Herng and X. Hai, *ACS Nano*, 2021, **15**, 7105-7113.

25. B. Martín-García, D. Spirito, S. Bellani, M. Prato, V. Romano, A. Polovitsyn, R. Brescia, R. Oropesa-Nuñez, L. Najafi, A. Ansaldo, *Small*. 2019, **15**, 1904670.

26. P. Guo, Z. Wang, T. Zhang, C. Chen, Y. Chen, H. Liu, M. Hua, S. Wei, X. Lu, *Appl. Catal. B: Environ. Energ*y, 2019, **258**, 117968.

27. H. Zhang, Q. Jiang, J. H. Hadden, F. Xie, D. J. Riley, *Adv. Energy Mater.* 2021, **31**, 2008989.

28. X. Zhou, Y. Zi, L. Xu, T. Li, J. Yang, J. Tang, *Inorg. Chem.* 2021, **60**, 11661.

29. Z. Zhang, X. Zhao, S. Xi, L. Zhang, Z. Chen, Z. Zeng, M. Huang, H. Yang, B. Liu, S. J. Pennycook, *Adv. Energy Mater.* **2020**, 10, 2002896.

30. T. Meng, Y.-N. Hao, L. Zheng, M. Cao, *Nanoscale* **2018**, 10, 14613.

31. W. Liao, W. Li, Y. Zhang, *Mater. Today Chem.* **2022**, 24, 100791.

32. X. Gao, H. Zhang, Q. Li, X. Yu, Z. Hong, X. Zhang, C. Liang, Z. Lin, *Angew. Chem. Int. Ed.* **2016**, 55, 6290.

33. H. Huang, S. Zhou, C. Yu, H. Huang, J. Zhao, L. Dai, J. Qiu, *Energy Environ. Sci.* **2020**, 13, 545.

34. J. Luo, J.-H. Im, M. T. Mayer, M. Schreier, M. K. Nazeeruddin, N.-G. Park, S. D. Tilley, H. J. Fan, M. Grätzel, *Sci.* **2014**, 345, 1593.

35. M. Ledendecker, S. Krick Calderón, C. Papp, H. P. Steinrück, M. Antonietti, M.

Shalom, *Angew. Chem. Int. Ed.* **2015**, 54, 12361.

36. L.-L. Feng, G. Yu, Y. Wu, G.-D. Li, H. Li, Y. Sun, T. Asefa, W. Chen, X. Zou, *J. Am. Chem. Soc.* **2015**, 137, 14023.